https://doi.org/10.3311/PPch.44147

Periodica Polytechnica Chemical Engineering

Autothermal Polarization of Membrane Electrode Assemblies – Effect of the Pt Content of the Catalyst and the Thickness of Fuel Cell Catalyst Layer

Balázs Kereszty[1], Gábor Pál Szijjártó[1*], Emese Lévai[2], Luka Szerb[1], Richárd Kunstár[1,3], András Tompos[1]

[1] Institute of Materials and Environmental Chemistry, HUN-REN Research Centre for Natural Sciences, POB 17, 1525 Budapest, Hungary
[2] Department of Energy Engineering, Faculty of Mechanical Engineering, Budapest University of Technology and Economics, Muegyetem rkp. 3., H-1111, Budapest, Hungary
[3] ArtTECHNICS Bt., Telepy street 5., 2nd floor / Nr.3, H-1096, Budapest, Hungary
[*] Corresponding author, e-mail: szijjarto.gabor@ttk.hu

Received: 30 March 2026, Accepted: 29 May 2026, Published online: 18 August 2026

Abstract

Laboratory-scale fuel cell testers typically regulate cell temperature via endplate heating cartridges. In practical stack applications, however, temperature control is achieved by cooling systems, making uniform temperature distribution a critical factor in system design and scale-up. To investigate these thermal effects under realistic conditions, autothermal activation and autothermal polarization experiments were conducted. Membrane electrode assemblies (MEAs) were polarized according to the New European Driving Cycle protocol, while galvanostatic electrochemical impedance spectroscopy (GEIS) measurements were performed in parallel to determine R_1, R_2, and C_2 parameters *in situ*. Three MEA configurations differing catalyst layers were tested: C-60-Pt, C-40-Pt, and C-60-Pt (0.13 mg Pt/cm^2), all with symmetrical Pt loadings. A custom-developed spray-gun robot was used for gas diffusion electrode fabrication. Among the samples, the C-40-Pt MEA demonstrated a pronounced break-in effect after 4 h of autothermal activation and achieved the highest current density. While the low-Pt MEA exhibited the lowest performance, it also showed the largest temperature rise during autothermal polarization. Impedance data confirmed that despite similar series resistance, the C-40-Pt MEA had lower internal resistance, while the more porous C-60-Pt showed increased R_1. More consistent curve shapes during autothermal conditions compared to fixed-temperature GEIS indicate that temperature adaptability enhances measurement reproducibility.

Keywords

proton exchange membrane fuel cell (PEMFC), spray-coating, autothermal, NEDC, GEIS, catalyst

1 Introduction

The increasing global population and energy demand have intensified research into alternative and sustainable energy conversion technologies [1, 2]. Among these, fuel cells have gained significant attention due to their high efficiency, scalability, and low emissions, producing only water as a by-product [3]. Fuel cells convert chemical energy directly into electrical energy using electrochemical reactions occurring at the anode and cathode [4], and they are considered promising alternatives to internal combustion engines, particularly in heavy-duty and large-scale transportation applications.

Among the various fuel cell types, proton exchange membrane fuel cells (PEMFCs) are the most widely applied due to their suitability for mobile and portable applications [5, 6]. Their operation relies on continuous supply of fuel and oxidant, while electrochemical reactions are facilitated by platinum-based electrocatalysts, typically carbon-supported platinum (Pt/C) [7]. However, the high cost of platinum and its critical role in performance make the optimization of catalyst layer composition and structure a key research challenge.

The performance of PEMFCs is strongly influenced by the properties of the membrane electrode assembly (MEA), including platinum loading, catalyst layer thickness, electrical resistance, and temperature-dependent behavior [8–13]. Previous studies have shown that both

Cite this article as: Kereszty, B., Szijjártó, G. P., Lévai, E., Szerb, L., Kunstár, R., Tompos, A. "Autothermal Polarization of Membrane Electrode Assemblies – Effect of the Pt Content of the Catalyst and the Thickness of Fuel Cell Catalyst Layer", Periodica Polytechnica Chemical Engineering, 2026.
https://doi.org/10.3311/PPch.44147

insufficient and excessive platinum loading can reduce efficiency due to limitations in catalytic activity and mass transport [14, 15]. Modeling results by Kulikovsky [16] further indicate that low Pt loading can deteriorate reactant transport and electrochemical performance. Since catalyst loading is proportional to catalyst layer thickness (assuming constant material properties), optimizing layer thickness is essential for balancing performance and material usage. As fuel cell performance is also affected by the activation procedure used prior to testing, representative activation protocols reported in the literature are summarized in Table 1 [17–22].

In addition to catalyst loading, the coupled effects of temperature and current density play a crucial role in PEMFC operation. Experimental studies have investigated these relationships under externally controlled conditions [23], while others have focused on self-heating effects and thermal shock behavior under operational conditions [24]. Furthermore, impedance-based diagnostic techniques, such as galvanostatic electrochemical impedance spectroscopy (GEIS), provide detailed insight into electrochemical processes, including ohmic resistance (R_1), charge transfer resistance (R_2), and double-layer capacitance (C_2) [25]. Studies have also demonstrated the dependence of these parameters on operating conditions such as humidity and reactant flow [25].

Beyond electrochemical properties, structural characteristics of the catalyst layer – such as thickness uniformity and porosity are critical for performance and durability. Thicker catalyst layers can hinder mass transport due to reduced diffusion rates, while excessively thin layers may not provide sufficient active sites for stable operation [26–28]. Although an optimal platinum concentration (e.g., 40 wt.% Pt/C) has been reported for maximizing power density [29], ensuring uniform catalyst distribution across the active surface remains essential to prevent local current density peaks and thermal hotspots, which can accelerate degradation [29–31].

Porosity is another key parameter, with an optimal value around 0.5 [32]. It can be defined as the ratio of total layer volume to platinum volume, as expressed in Eq. (1). Both low and high porosity values negatively affect performance by increasing diffusion losses or reducing electrochemically active surface area, respectively [33–35]. In addition, long-term degradation mechanisms, including carbon support oxidation, platinum dissolution, Ostwald ripening, and nanoparticle agglomeration, must be considered, as they significantly impact durability regardless of initial catalyst layer optimization.

$$P_t = \frac{V_t}{V_c} \times 100 \,, \tag{1}$$

where:

V_t: total volume of the material in the layer [m^3]

V_c: volume of the Pt in the layer [m^3]

P_t: porosity of the layer [-]

Beyond initial performance optimization, long-term durability of the catalyst layer must also be considered. For proper water management, the catalyst layer should be electrically conductive and exhibit a mesoporous structure. However, degradation processes strongly depend on the redox properties of the catalyst support and the stability of

Table 1 Some examples of activation protocols used in case of fuel cells to achieve the best output characteristics

Method description	Operating procedures and details	Ref
Constant current	The current density was maintained at 1 A/cm^2 for 6 h, during which the cell voltage stabilized, with fluctuations remaining within 1 mV.	[17]
Linear sweeps of current	Linear current sweeps were performed from 400 mA/cm^2 to 3.0 A/cm^2 in 50 mA/cm^2 increments, with each step lasting 5 min. This procedure was repeated four times to achieve optimal power density, taking approximately 18 h in total.	[18]
Constant voltage	25 h MEA conditioning procedure by controlling the current density and holding for 5 h at 50, 200, 500, 800, and 1000 mA/cm^2, respectively	[19]
	Fixed voltage (e.g., 0.6 V) for hours	[20]
High current pulse activation	Rectangular current pulses at 1.3 times the rated maximum current, each lasting 10 s with 60 s rest intervals	[21]
Amperometric pulsed activation	Repeated pulsed loading cycles – 10 to 80 s at 0.1 V load followed by 20 to 40 s of open-circuit rest – over a total duration of 3 h	[22]
Amperometric conditioning	Linear current sweeps from 2 A (400 mA/cm^2) to 15 A (3.0 A/cm^2) with 0.25 A (50 mA/cm^2) steps, each held for 5 min. The procedure was repeated 4 times until the difference between the last two scans was <50 mA. Total conditioning time: ~18 h. Full MEA activation confirmed by power density stabilization.	[18]

the active phase too. In the case of carbon-supported catalysts, carbon oxidation can occur at high cathode potentials, leading to the detachment of platinum nanoparticles from the support. Furthermore, additional degradation mechanisms such as platinum dissolution, Ostwald ripening, and particle agglomeration contribute to the gradual loss of electrochemically active surface area and overall performance decline. These degradation phenomena must be evaluated independently of catalyst layer thickness, and comparisons should be performed under identical operating conditions, particularly at the same current density, to ensure meaningful interpretation of results. This highlights the importance of controlled experimental methodologies when investigating catalyst layer behavior.

In addition to degradation, achieving uniform catalyst layer thickness is particularly critical at low platinum loadings [36, 37]. Although carbon-supported platinum catalysts currently provide the best balance between performance and stability in PEMFCs, their high cost necessitates minimizing material losses during MEA fabrication [38]. To address this challenge, the spray-coating device developed and applied in this study enables highly uniform and precise deposition of catalyst layers, even at low Pt content. This approach provides a cost-effective solution at laboratory scale while maintaining scalability for larger-scale applications.

Despite extensive research on catalyst layer design and PEMFC performance, limited attention has been paid to the interplay between catalyst loading, autothermal behavior, and electrochemical impedance characteristics during activation and operation. In particular, the relationship between self-heating phenomena and fundamental electrochemical processes (such as proton conduction, charge transfer, and double-layer formation) remains insufficiently understood. To address this gap, this study investigates autothermal effects in PEMFC catalyst layers with varying platinum loadings.

The high-precision spray-coating method is used also to produce uniform catalyst layers with controlled Pt content, minimizing material loss during MEA fabrication. The evolution of temperature during activation and under electrical load is analyzed and correlated with electrochemical processes identified using GEIS measurements. Specifically, the study examines the relationship between ohmic resistance (R_1), charge transfer resistance (R_2), double-layer capacitance (C_2), current density j, and autothermal temperature.

$$C_2 = \frac{1}{-Im_{\max} \times 2\pi \times \text{frequency} \times R_2}, \quad (2)$$

where $Im_{\max}$ is the maximal value of imaginary part.

The findings contribute to a deeper understanding of the coupling between thermal and electrochemical phenomena in PEMFCs and provide insights for optimizing catalyst layer design. This work supports the development of a 500 W small-scale PEMFC stack for vehicle or drone applications, where precise control of platinum loading is essential for achieving optimal performance and cost-efficiency, particularly in relation to balance-of-plant components such as thermal management systems.

2 Methods

2.1 Materials

The study compared MEAs with three different catalyst layer configurations, focusing on variations in both platinum content of the applied carbon supported 40 and 60 wt.% Pt/C catalysts (C-40-Pt and C-60-Pt, respectively; C: Vulcan XC-72 product, QuinTech [39]) and Pt loading of the catalyst layer on the gas diffusion electrode (GDE) (in mg Pt/cm^2). The tested MEA configurations included: C-40-Pt with 0.57 mg Pt/cm^2, and C-60-Pt with 0.57, and 0.13 mg Pt/cm^2 Pt loading. These Pt loadings were applied symmetrically; each MEA had the same Pt loading on the cathode and anode sides. Proton exchange membrane (PEM) of the tested MEAs was Nafion® XL [40], which was purchased from Ion Power Ltd., Germany. Gas diffusion layers (GDLs) were prepared using teflon loaded H23C6 carbon paper (Freudenberg FCCT, Germany). For the sake of simplicity, the catalysts will be denoted in the figures according to the abbreviations introduced in Table 2.

2.2 Manufacturing of membrane electrode assemblies and cell composition

Each MEA had an active surface area of 16 cm^2. Gas diffusion electrodes were made by spray-coating. Table 3 presents the detailed composition of the catalyst ink (where m_{catalyst} is the mass of the used catalyst, V_{ionomer} is the used volume of ionomer, V_{solvent} is the used solvents volume, IPA means isopropanol, and I/C ratio means

Table 2 Definition of samples

Name	Short name
C-60-Pt loading = 0.57 [mg/cm^2]	P
C-60-Pt loading = 0.13 [mg/cm^2]	Q
C-40-Pt loading = 0.57 [mg/cm^2]	R

Table 3 Composition of the catalyst ink (detailed in Section 2 of Supplement)

Short name	Catalyst type	$m_{catalyst}$ [mg]	$V_{ionomer}$ Nafion [mL]	$V_{solvent}$ IPA [mL]	I/C ratio
P	C-60-Pt	105.56	1.125	2.815	0.5
Q	C-60-Pt	52.78	0.565	1.405	0.5
R	C-40-Pt	185.55	1.98	5.935	0.5

ionomer/carbon ratio). The applied ionomer was a 5 m/m% Nafion solution (DuPont, United States), while analytical grade isopropanol (MolarChem, Hungary) was used as the solvent. The dry Nafion to catalyst mass ratio was 0.5. The catalyst ink was mixed at room temperature for 2 h using a magnetic stirrer. A home-made spray-gun robot (see Fig. 1) was developed for this purpose by ArtTECHNICS Bt. (Hungary). Moving of the nozzle (Krautzberger, Germany) MikroXS, 0.2 mm inner diameter was regulated by G-code program. The blowing distance between the carbon paper and the nozzle was fixed to 70 mm. Ready GDEs were heat treated at 85 °C for 30 min and then at 120 °C for 30 min. GDEs were built together with PEM by hot pressing for 3 min at 120 °C with 270 MPa pressure. For exact temperature measurement, a 0.25 mm diameter Type K thermocouple (RHODIUM Kft., Hungary) was inserted into the MEAs, between the proton exchange membrane and the gasket. In the experimental cell Ti bipolar plates (BPPs) with single serpentine gas flow channels were applied (made by ArtTECHNICS Bt). The pulling torque of the bolts (8 pc., 6 mm diameter) of the cell endplates was 4 Nm.

In the context of porous PEMFC catalyst layers, defining an exact geometric thickness is not meaningful due to their nanoscale roughness, heterogeneous porosity, and irregular morphology. Surface techniques such as scanning electron microscopy (SEM) or profilometry cannot capture a single, unambiguous thickness value. Therefore, performance differences are more reliably attributed to structural and compositional parameters such as Pt loading, ionomer content, and electrochemically active surface area (ECSA), rather than to a poorly defined layer thickness [41, 42].

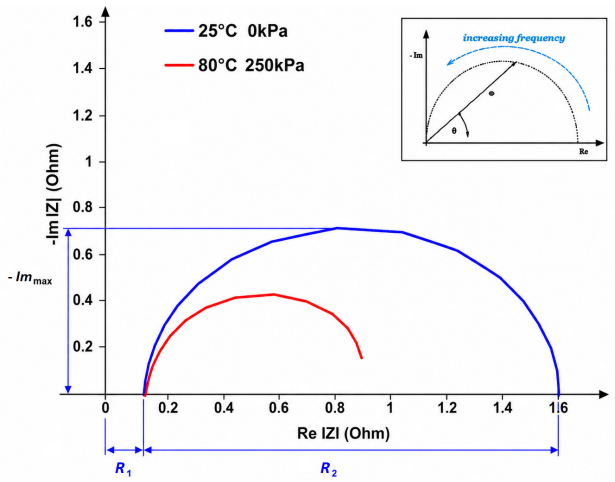

Fig. 1 Explanation of used terms R_1, R_2 and C_2. In fuel cell impedance models, R_1 is the ohmic resistance of the membrane and contacts, R_2 is the charge transfer resistance describing electrode reaction kinetics, and C_2 is the double-layer capacitance representing charge separation at the electrode–electrolyte interface. More detailed explanation can be seen in Fig. S1.

The differentiation between the effects of catalyst layer thickness and platinum content on temperature behaviour is discussed in detail in Section 2 of Supplement. The methodology used for calculating the Tafel slope of the MEAs is described in detail in Section 3 of Supplement.

2.3 Autothermal activation

A 850 Fuel Cell Test System (Scribner, Germany) was used to measure the autothermal activation of the MEAs. The activation lasted for 12 h (as reported by Du et al. [43]), during which increases in current and temperature were monitored. No external heating was applied, and measurements began at a cell temperature of 25 °C. Humidifiers were kept continuously at 25 °C both on cathode and anode. Back pressures were 150 kPa (H_2) at the anode and 130 kPa (O_2) at the cathode. The flow rates of hydrogen (anode) and oxygen (cathode) were 200 mL/min. The detailed explanation can be find in Section 4 in Supplement.

Fuel cell testing followed the New European Driving Cycle (NEDC) protocol with defined conditions (80 °C, controlled humidity, and specified back pressures), ensuring comparability with other studies. During autothermal activation the pressures were reduced due to room-temperature operation and polyethylene gasket limitations, while a pressure difference between anode and cathode was maintained to prevent water crossover. The more detailed rationale behind the use of different anode and cathode back pressures during autothermal activation is detailed in Section 4 of Supplement.

2.4 Autothermal polarization and impedance spectroscopy with galvanostatic electrochemical impedance spectroscopy supplement

The conditions were the same as in case of autothermal activation. The most important difference was that in this case the voltage was measured and the current was increased in

steps of 1 A / 10 min. Analysis was combined with GEIS in order to understand the changes in processes occurring in the cell during polarization. In GEIS measurements, the given electrical load (current) is perturbed with an alternating current of constant amplitude of 500 mA, and the voltage response is recorded in a wide frequency range of 1–10,000 Hz. This technique provides detailed information on the internal resistive and capacitive properties of the cell. The results are commonly analyzed using Nyquist plots and equivalent circuit models, allowing parameters such as R_1, R_2, and C_2 to be determined (see Fig. S1 in the Supplement).

The load step durations applied during the polarization protocols were as follows:

- For standard NEDC (according to NEDC regulation, according to the load-dependent) polarization, a step duration of 2 min was used.
- For voltage-current galvanistatic electrochemical impedance spectroscopy (UI-GEIS) measurements at fixed temperature (polarization combined with impedance spectroscopy), each step lasted for 5 min.
- In the autothermal (without external heating, heating dictated by cell reaction kinetics) UI-GEIS protocol, a step duration of 10 min was implemented to ensure adequate thermal stabilization by the end of each current level, allowing for reliable acquisition of the impedance spectra. This timing was established based on prior empirical experience.

2.5 Polarization with impedance spectroscopy at 80 °C

As references for the autothermal case, the polarizations were repeated in case of all MEAs at fixed cell temperature (T = 80 °C), where relative humidity were also constant (50% on anode, 30% on cathode). Measurement parameters were based on the basic polarization settings of the NEDC protocol [44]. Accordingy, the back pressure value at the anode was 250 kPa and at the cathode was 230 kPa. NEDC is an EU-harmonized protocol for PEMFC MEA testing, and is therefore suitable for us as an internationally accepted reference. In these polarizations, GEIS was also measured in each current step (1 A / 5 min). GEIS settings have not changed (1–10,000 Hz, amplitude: 500 mA). NEDC protocol offers 2 min steps, but according to our experience, 5 min steps resulted in better current stability. Right before NEDC polarization, the MEAs were held at 400 mV for 90 min under the measurement conditions. This "second activation" was necessary to equilibrate the initial state of the MEAs, which had changed due to the prior autothermal measurements.

In a single cell arrangement, fuel cell testers usually control the temperature of the cell by heating cartridges inserted into the endplates. This is the laboratory scale solution. However, in practice, other method has to be found to ensure even temperature distribution. External cooling is necessary due to the exothermic nature of the cell processes. To design an appropriate cooling solution for a stack, as part of the Balance of Plant (BoP), we have to study and understand the autothermal phenomena. Closed cathode PEMFC stacks can be cooled by air or by liquid. There is an optimal cell temperature that results in the highest possible power density while avoiding damage to the membranes.

3 Results and discussion

As can be seen from Fig. 2(a), during autothermal polarization, the MEA containing 60 wt.% Pt/C at a loading of 0.57 mg Pt/cm^2 (sample P) showed a slightly higher initial voltage (open circuit voltage) than the MEA containing 40 wt.% Pt/C at the same Pt loading (sample R). During the autothermal polarization (Fig. 2(a)), it was observed that in both the activation polarization and ohmic polarization regions, the MEAs with higher platinum loading in the GDE (0.57 mg Pt/cm^2, sample P and R) demonstrated nearly identical performance, both exceeding the cell performance measured on the MEA with lower platinum loading (0.13 mgPt/cm^2, sample Q). At higher current densities, approaching the concentration polarization region, the MEA prepared with 40 wt.% Pt/C increasingly outperforms that prepared with 60 wt.% Pt/C. In this region, the MEA with lower platinum content still lags behind in performance, but the difference is smaller compared to that observed in the activation polarization region (Fig. 2(a)).

As reference, we performed the polarization process according to the unified standard NEDC protocol (Fig. 2(b)). Similarly to autothermal polarization, MEAs with higher Pt content perform better than the MEA with lower Pt content in the entire region of the polarization curve. There is no significant difference between the two MEAs containing 0.57 mg/cm^2 Pt loading, with increasing current density, the MEA containing 40 wt.% Pt/C catalyst slightly outperforms the MEA prepared using 60 wt.% Pt/C. Fig. 2(c) shows that the MEA containing 60 wt.% Pt/C at a loading of 0.13 mg Pt/cm^2 (sample Q) has the highest temperature at all measured current density points. This observation is in good agreement with the lower electrical efficiency of the sample over the entire range of the polarization curve, which therefore also implies a more pronounced heat loss.

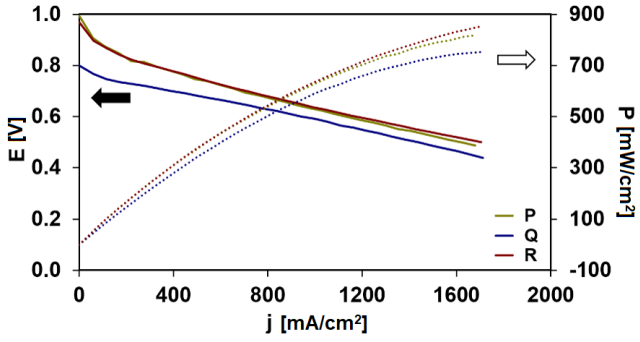

(a)

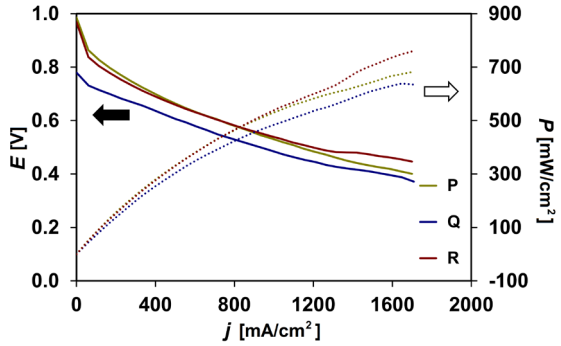

(b)

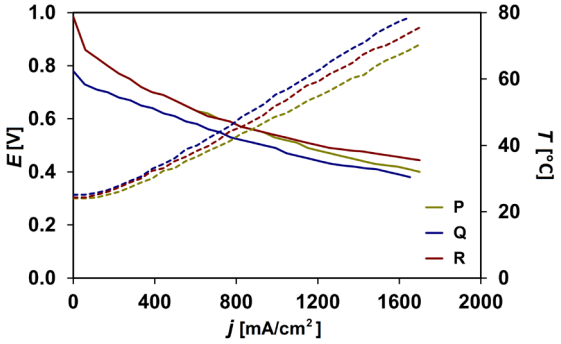

(c)

Fig. 2 (a) Autothermal and (b) NEDC polarization curves and (c) the temperature evolution in autothermal polarization

These results are in good agreement with the simulations by Carcadea et al. [45], who found that the lower Pt content in the activation polarization region significantly reduces the cell performance, and also explains why the 40 wt.% Pt/C catalyst performs slightly better at higher currents with the same Pt content. Carcadea et al.'s simulations refer to the phenomenon of faster mass transport in this case.

An equivalent circuit model [46] was fitted for GEI spectra recorded in autothermal polarization. The points of the autothermal measurement taken at 1 A/cm^2 are also shown separately in Table 4, that is an extract of the more detailed diagram group in Section 5 of Supplement. Analyzing the R_1, R_2 and C_2 values obtained (Fig. 3 and

Table 4 Equivalent circuit model for autothermal polarization. Ohmic resistance (R_1), charge transfer resistance (R_2) and capacitance C_2 at 1 A/cm^2 current density

Sample	E [V]	R_1 [Ω × cm²]	R_2 [Ω × cm²]	C_2 [F/cm²]	T [°C]
P	0.0330	0.0128	0.0080	0.00086	48.76
Q	0.0303	0.0144	0.0096	0.00039	55.50
R	0.0336	0.0112	0.0112	0.00117	52.13

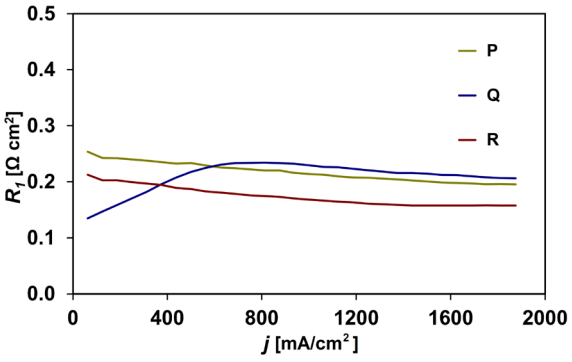

(a)

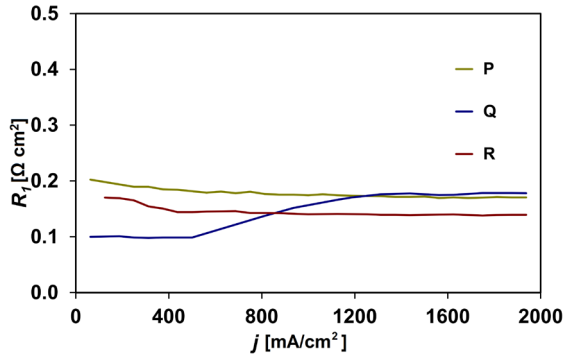

(b)

Fig. 3 R_1 values obtained in (a) autothermal polarization and (b) in NEDC measurements. Data of R_2 and C_2 can be find in Section 5 of Supplement.

Fig. S2 in the Supplement), in the case of MEA containing 60 wt.% Pt/C at a loading of 0.13 mg Pt/cm^2 (sample Q) we can see that with increasing current density, the C_2 value initially decreased and then remained fairly constant. The C_2 value refers to the double-layer capacitance of the electrode-electrolyte interfaces. It appears that the contact between Nafion and Pt/C catalyst particles weakens in the ohmic and concentration polarization regions. In the case of autothermal polarization, with increasing current density, the relative humidity of the gases reaching the electrodes continuously decreases, meaning that we can expect the Nafion ionomer in the membrane and the catalyst layer to dry out. Shrinkage of the Nafion ionomer due to water loss can lead to a decrease in the interfacial

area between the catalysts and Nafion. This phenomenon is consistent with the increase in ohmic resistance (R_1 in Fig. S2 in the Supplement for sample Q in the autothermal polarization case), which can practically be attributed to the increase in the resistance of the ion exchange membrane between the electrodes. Ohmic resistance appears as a single point on the x-axis of the Nyquist plot at high frequencies. The Nyquist plots of sample P can be seen in Fig. 4, the other two sample's detailed results are in Fig. S3. These results show that the ohmic resistance of sample P is fairly constant or even slightly decreases, while for sample Q there is a pronounced increase in R_1 with increasing current densities.

The narrowing of performance differences between membrane electrode assemblies with different platinum loadings in the concentration polarization region can be attributed to the increasing dominance of mass transport and water management limitations during autothermal operation. At elevated current densities, oxygen transport to the cathode becomes the rate-limiting factor, while excess liquid water accumulation in the catalyst and gas diffusion layers further restricts reactant access. Under these conditions, the kinetic advantages associated with higher platinum loading are progressively masked, leading to convergence of cell performance regardless of catalyst content. This behavior is reflected in the polarization curves, where voltage losses in the high current density regime are governed primarily by mass transport effects rather than catalytic activity [47, 48].

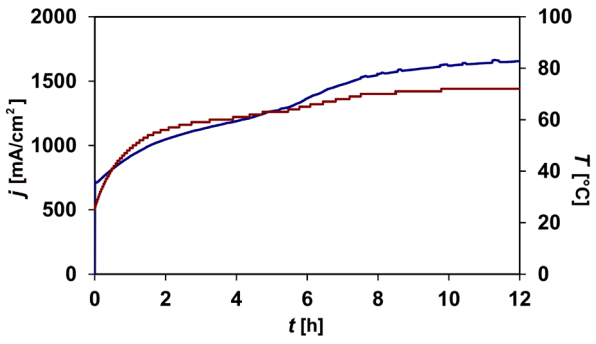

(a)

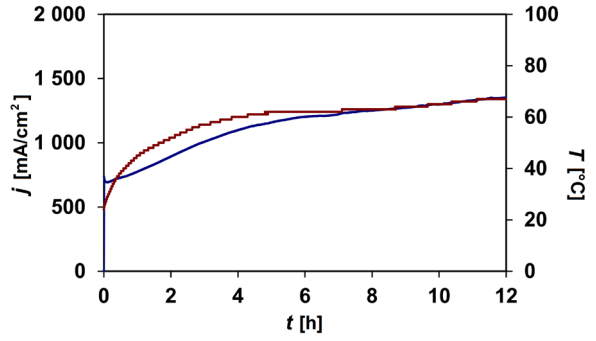

(b)

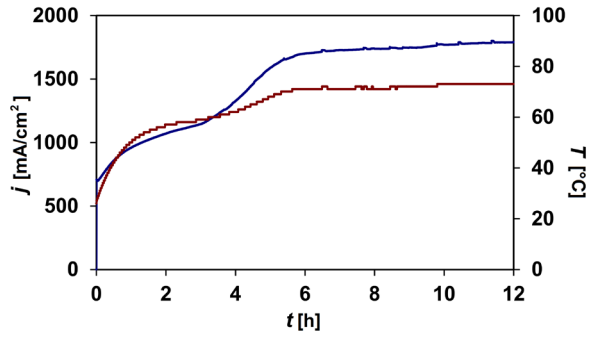

(c)

Fig. 4 Hange of current density and temperature with time in case of autothermal activation: (a) sample P, (b) sample Q, (c) sample R

Under autothermal polarization conditions, the cell temperature increases with current density due to the exothermic nature of the electrochemical reaction. This temperature rise enhances membrane proton conductivity, which can outweigh the effect of decreasing inlet gas relative humidity, resulting in a net decrease in ohmic resistance. Therefore, the observed trend – lower ohmic resistance at higher current densities – is primarily attributed to temperature-driven improvements in membrane ionic conductivity rather than humidity effects alone [49–51].

In case of autothermal polarization the most important difference from a simple polarization is that there are two competitive processes: i) increasing of the temperature (because of the increasing of the current) increases the performance of the cell; ii) because of that the cell temperature is increasing, but the temperature of the humidifiers is not changing, relative humidity are continously decreasing, which have a negative effect on the power of the cell. Experiments showed, that the effect of the temperature is stronger, and because of that, the power of the cell was increasing. It is detailed in Section 5 of Supplement.

The double layer capacitance was the highest for MEA containing 40 wt.% Pt/C at a loading of 0.57 mg Pt/cm^2 (in Fig. S2 in the Supplement for sample R in the autothermal polarization case). The 40 wt.% Pt/C catalyst has a higher Brunauer-Emmett-Teller (BET) surface area than the 60 wt.% Pt/C catalyst, eventually resulting in greater interfacial contact between the Nafion ionomer and the catalyst particles and thus sample R exhibited the highest double-layer capacitance.

Charge transfer resistance characterizes the electrocatalytic reactions in a MEA. Theoretically, both the anodic and cathodic processes, i.e. hydrogen electrooxidation (HOR) and oxygen reduction reaction (ORR), can

be evaluated with GEIS, but since ORR is kinetically more hindered, the charge transfer resistance is more pronounced in the case of ORR, and the HOR process is practically undetectable. Fig. S2 in the Supplement shows a monotonic decrease in R_2 values for all samples, which is consistent with the fact that during autothermal polarization, the temperature increases monotonically due to the increasing current density, which naturally results in improved reaction kinetics.

Interestingly, the samples with a Pt content of 0.57 mg Pt/cm^2 (sample P and R) have a higher charge transfer resistance than the sample with a Pt content of 0.13 mg Pt/cm^2 at low current densities, i.e. close to open circuit voltage. Indeed, this observation is consistent with the sudden decrease in voltage in the activation polarization region in the polarization curves of high Pt-content samples.

Additional remarks concerning porosity and electrochemically active surface area, including a discussion of the limitations in corresponding characterization data, are provided in Section 8 of Supplement.

In the activation polarization region, the effect of temperature is superimposed on the effect of overvoltage according to the Tafel equation. Note: the overvoltage has a linear correlation with the logarithm of the current density, and the slope of this relationship (Tafel slope) depends on the ORR reaction mechanism [52]. A steeper Tafel slope is expected if the rate-determining step is the first, proton-coupled charge transfer, while if subsequent charge transfer steps are the rate-determining, the Tafel slopes are smaller. For MEAs with high Pt content, the amount of proton exchange sites relative to Pt content is smaller than for MEA with low Pt content, which ultimately would lead to the first proton coupled charge transfer ORR step as rate determining in case of P and R samples.

Fig. 4 shows the time dependence of the autothermal activation. It can be seen that the current density change obtained on the higher Pt content MEAs (sample P and R) occurred at a nearly identical rate and reached the same final current densities within 12 h. In contrast, for MEA with lower Pt content, higher self-heating temperatures and correspondingly lower current densities were measured over the same amount of time.

Analyzing the GEIS measurements shown in Fig. 5(b) and Fig. S8 in Supplement using the equivalent circuit model, it can be concluded that the changes in the parameters R_1, R_2, and C_2 obtained for the polarization according to the NEDC protocol showed similar trends as in

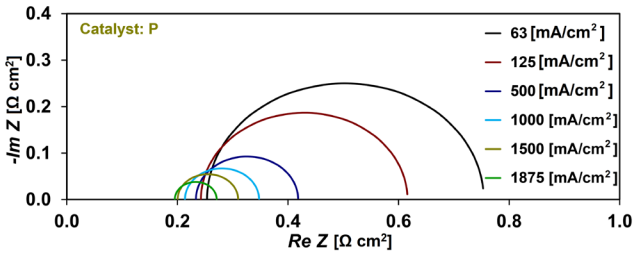

(a)

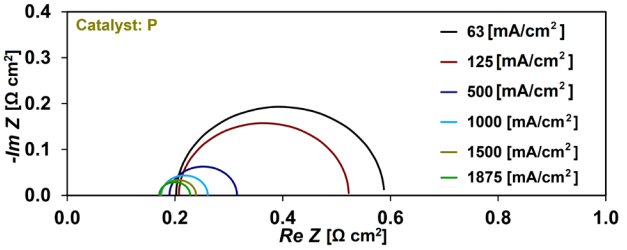

(b)

Fig. 5 (a) GEIS curves from autothermal polarization and (b) at 80 °C constant temperature. The corresponding diagrams for the samples Q and R can be found in Section 6 of Supplement.

the autothermal measurements, the extract of measurement is in the Table 5. As it can be seen in the Fig. S5 in Supplement, the MEA containing 40 wt.%Pt/C at a loading of 0.57 mg Pt/cm^2 (sample R) showed lower ohmic resistance over the entire range of current densities compared to sample P. As discussed above, this can be attributed to too excessive porosity of 60 wt.% Pt/C [53] compared to that of the 40 wt.% Pt/C catalyst, which ultimately leads to smaller electrochemically active surface area and higher contact resistance. This experimentally confirms the calculations of Kriston and Popov [54]. In their studies, porosimetry measurements showed that at higher Pt concentrations, the agglomerates become larger, the pore size changes from below 10 nm to around 40 nm and the proportion of small pores decreases. This suggests that newly deposited particles cover previously deposited particles and reduce the available catalytic surface area.

For the sample with 0.13 mg/cm^2 Pt loading (sample Q), similarly to autothermal case, R_1 values increased again. It seems that the low rate of the cathodic ORR process

Table 5 Equivalent circuit model for NEDC polarization. Ohmic resistance (R_1), charge transfer resistance (R_2) and capacitance C_2 at 1 A/cm^2 current density

NEDC polarization, 80 °C, 250–230 kPa, relative humidity 50–30%				
Sample	E [V]	R_1 [Ω × cm^2]	R_2 [Ω × cm^2]	C_2 [F/cm^2]
P	0.0393	0.0112	0.0048	0.00094
Q	0.0369	0.0096	0.0048	0.00041
R	0.0340	0.0080	0.0064	0.00116

does not provide enough water for proper hydration of either the membrane between the GDEs or the ionomer around the catalyst particles, although in the NEDC protocol polarization the relative humidity of the gases is uniform over the entire range of current densities.

The charge transfer resistance values (R_2) obtained during NEDC polarization at low current densities follow the trends known from the autothermal case. Accordingly, the difference between the initial charge transfer resistance values for different samples can be attributed to difference in the ORR mechanism. The first proton-coupled charge transfer step may be the rate-determining step for samples with high Pt content (P and R), while for the sample with a thin catalyst layer, the subsequent charge transfer may be the rate-determining step. At low current densities, the largest decrease in R_2 is again associated with the P and R samples. However, at higher current densities, we can observe a stabilization of these values, or at least the slope of the further decrease is significantly smaller than in the autothermal case. Namely, in the case of polarization performed at a constant temperature, we can only expect the effect of overvoltage on electrocatalytic reactions, according to Tafel equation. There is no temperature change that affects the charge transfer resistance as in the case of autothermal polarization.

In the NEDC polarization, a rather hectic fluctuation in the double-layer capacitance (C_2) is observed. This is in good agreement with simulation results by Halvorsen et al. [55], which showed that GEIS measurements at fixed temperatures show high variance. This effect is more pronounced at lower Pt loadings.

4 Conclusion

In the case of MEAs with high Pt content, i.e. thick catalyst layers, the Pt concentration of the catalyst is important. The MEA made of 40 wt.% Pt/C outperforms the MEA made with a higher-Pt content catalyst (60 wt.% Pt/C) at high current densities. It has been confirmed that too high porosity of 60 wt.% Pt/C compared to that of the 40 wt.% Pt/C catalyst decreased the electrochemical active surface area and increased the ohmic resistance of the MEA. In addition, the surface area of the 40 wt% Pt/C catalyst exceeds that of the 60 wt% Pt/C catalyst, ultimately resulting in an extended interface between the Nafion ionomer and the catalyst particles, so the MEA sample made of the 40 wt%Pt/C catalyst showed the highest double-layer capacitance.

The use of too thin catalyst layer has several disadvantages in the case of autothermal polarization. First, the ORR reaction cannot adequately support the water management of MEA because relatively little water is generated, leading to shrinkage of the Nafion ionomer due to water loss, resulting in a decrease in the interfacial area between the catalysts and Nafion. Eventually, both the double-layer capacitance and proton conductivity of the MEA decrease, leading to lower efficiency over the entire current density range of the polarization curve. Low electrical efficiency also means high heat loss. As a result, the autogenic temperature developed during autothermal activation and polarization exceeds the temperature of MEAs made with thicker catalyst layers.

Acknowledgement

This research was funded by Project no. RRF-2.3.1-21-2022-00009, titled the National Laboratory for Renewable Energy, and has been implemented with the support provided by the Recovery and Resilience Facility of the European Union within the framework of Programme Széchenyi Plan Plus.

We wish to express our special thanks to Dr. Irina Borbáth and for Dr. Tamás Pajkossy.

We dedicate this work to the memory of Dr. István Kovács (Labornite Kft.).

Prepared with the professional support of the Cooperative Doctoral Program of the University Research Scholarship Program of the Ministry of Culture and Innovation Financed from the National Research, Developmant and Innovation Found.

References

[1] Shafiullah, M., Ahmad, M., Awda, Y., Maaruf, M., Ali, M. O., AlShumayri, K. A., Rahman, S. M. "Hydrogen to Power: Exploring Current Developments and Future Challenges", Natural Sciences, 6(3), e70070, 2026. https://doi.org/10.1002/ntls.70070

[2] Fuel Cell Electric Buses "About Fuel Cell Electric Buses", Hydrogen Europe and WaterstofNet, Slachthuisstraat, 2023.

[3] Reaves, W., Hoberecht, M. "Proton Exchange Membrane (PEM) Fuel Cell Status and Remaining Challenges for Manned Space-Flight Applications", In: 1st International Energy Conversion Engineering Conference (IECEC), Portsmouth, VA, USA, 2003, pp. 1–7. https://doi.org/10.2514/6.2003-5963

[4] Viswanathan, B., Scibioh, M. A. "Fuel Cells: principles and applications", CRC Press LLC: Taylor and Francis Group, 2007. ISBN 978 1 4200 6028 7

[5] Peighambardoust, S., Rowshanzamir, S., Amjadi, M. "Review of the proton exchange membranes for fuelcell applications", International Journal of Hydrogen Energy, 35(17), pp. 9349–9384, 2010. https://doi.org/10.1016/j.ijhydene.2010.05.017

[6] Kurnia, J., Sasimoto, A. "Hydrogen fuel cell in vehicle propulsion: performance, efficiency, and challenge", In: Sulaiman, S. A. (ed.) Energy Efficiency in Mobility Systems, Springer Singapore, 2020, pp. 9–26. ISBN 978-981-15-0102-9 https://doi.org/10.1007/978-981-15-0102-9_2

[7] Zhao, Y., Mao, Y.., Zhang, W., Tang, Y., Wang, P. "Reviews on the effects of contaminations and research methodologies for PEMFC", International Journal of Hydrogen Energy, 45(43), pp. 23174–23200, 2020. https://doi.org/10.1016/j.ijhydene.2020.06.145

[8] Appleby, A. J., Foulkes, F. R. "Fuel cell handbook", Van Nostrand Reinhold, 1989. ISBN 9780442319267

[9] Kaur, G. (ed.) "PEM fuel cells: fundamentals, advanced technologies, and practical application", Elsevier, 2021. ISBN 978-0-12-823708-3

[10] Sadiq Al-Baghdadi, M. A. R. "A simple mathematical model of performance for proton exchange membrane fuel cells", International Journal of Sustainable Energy, 26(2), pp. 79–90, 2007. https://doi.org/10.1080/14786450701549840

[11] Zagoraiou, E., Paloukis, F., Neophytides, S. G., Daletou, M. K. "The electrochemical interface of the cathode in high temperature PEM fuel cells", Electrochimica Acta, 356, 136778, 2020. https://doi.org/10.1016/j.electacta.2020.136778

[12] San, F. G. B., S. Dursun, S., Yazici, M. S. "PtCo on continuous-phase graphene as PEM fuel cell catalyst", International Journal of Energy Research, 45(2), pp. 1673–1684, 2002. https://doi.org/10.1002/er.5830

[13] Sulaiman, M., Hannan, M. A., Mohamed, A., Majlan, E. H., Daud, W. R. "A review on energy management system for fuel cell hybrid electric vehicle: Issues and challenges", Renewable and Sustainable Energy Reviews, 52, pp. 802–814, 2015. https://doi.org/10.1016/j.rser.2015.07.132

[14] Alink, R., Singh, R., Schneider, P., Christmann, K., Schall, J., Keding, R., Zamel, N. "Full Parametric Study of the Influence of Ionomer Content, Catalyst Loading and Catalyst Type on Oxygen and Ion Transport in PEM Fuel Cell", Molecules, 25(7), 1523, 2020. https://doi.org/10.3390/molecules25071523

[15] Ahn, C.-Y., Kim, S., Choi, H. J., Lee, J., Kang, S. Y., …, Cho, Y.-H. "Effect of iridium oxide as an additive on catalysts with different Pt contents in cell reversal conditions of polymer electrolyte membrane fuel cells", International Journal of Hydrogen Energy, 47(3), pp. 1863–1873, 2022. https://doi.org/10.1016/j.ijhydene.2021.10.226

[16] Kulikovsky, A. "The effect of Nafion film on the cathode catalyst layer performance in a low–Pt PEM fuel cell", Electrochemistry Communications, 103, pp. 61–65, 2019. https://doi.org/10.1016/j.elecom.2019.05.003

[17] Xie, Z., Zhao, X., Adachi, M., Shi, Z., Mashio, T., Ohma, A., Shinohara, K., Holdcroft, S., Navessin, T. "Fuel cell cathode catalyst layers from "green" catalyst inks", Energy & Enviromental Science, 1(1), pp. 184–193, 2008. https://doi.org/10.1039/B808613N

[18] Balogun, E., Barnett, A. O., Holdcroft, S. "Cathode starvation as an accelerated conditioning procedure forperfluorosulfonic acid ionomer fuel cells", Journal of Power Sources Advances, 3, 100012, 2020. https://doi.org/10.1016/j.powera.2020.100012

[19] Bi, W., Gray, G. E., Fuller, T. F. "PEM Fuel cell Pt/C Dissolution and Deposition in Nafion Electrolyte", Electrochemical and Solid-State Letters, 10(5), pp. B101–B104, 2007. https://doi.org/10.1149/1.2712796

[20] Taghiabadi, M. M., Zhiani, M. Silva, V. "Effect of MEA activation method on the long-term performance of PEM fuel cell", Applied Energy, 242, pp. 602–611, 2019. https://doi.org/10.1016/j.apenergy.2019.03.157

[21] Wang, D., Ding, X., Yang, D., Liang, Z., Wang, L. "A novel high current pulse activation method for proton exchange membrane fuel cell", AIP Advances, 11(5), pp. 570–573, 2021. https://doi.org/10.1063/5.0046879

[22] Galitskaya, E. A., Gerasimova, E. V., Dobrovol'skii, Y. A., Don, G. M., Afanas'ev, A. S., Levchenko, A. V., Sivak, A. V., Sinitsyn, V. V. "Pulsed Activation of a Fuel Cell on the Basis of a Proton-Exchange Polymer Membrane", Technical Physics Letters, 44(7), pp. 570–573, 2018. https://doi.org/10.1134/S1063785018070064

[23] Yang, Z., Wang, R., Hao, D., Wu, K., Liang, J., Wu, S., Ma, M., Du, Q., Zhang, Y. "Investigation of current density and temperature distribution characteristics under transient conditions based on a 108 cm^2 segmented proton exchange membrane fuel cell", International Journal of Hydrogen Energy, 80, pp. 125–136, 2024. https://doi.org/10.1016/j.ijhydene.2024.07.043

[24] Koh, J.–H., Hsu, A. T., Akay, H. U.., Liou, M.-F. "Analysis of overall heat balance in self-heated proton-exchangemembrane fuel cells for temperature predictions", Journal of Power Sources, 144(1), pp. 122–128, 2005. https://doi.org/10.1016/j.jpowsour.2004.12.055

[25] Pivac, I., Šimić, B., Barbir, F. "Experimental diagnostics and modeling of inductive phenomena at low frequencies in impedance spectra of proton exchange membrane fuel cells", Journal of Power Sources, 365, pp. 240–248, 2017. https://doi.org/10.1016/j.jpowsour.2017.08.087

[26] Xia, L., Ni, M., Xu, Q., Xu, H., Zheng, K. "Optimization of catalyst layer thickness for achieving high performance and low cost of high temperature proton exchange membrane fuel cell", Applied Energy, 294, 117012, 2021. https://doi.org/10.1016/j.apenergy.2021.117012

[27] Jiang, Z., Yang, G., Shen, Q., Li, S., Liao, J., Yang, X., Sun, J. "Liquid water transport phenomena in the porous transport layer of proton exchange membrane fuel cell based on lattice Boltzmann simulation", Materials Today Communications, 37, 107633, 2023. https://doi.org/10.1016/j.mtcomm.2023.107633

[28] Li, S., Chen, P.., Zhang, S., Jiang, Z., Liao, J., Gao, P., Shen, Q. "The mass transport and electrochemical reaction in the cathode catalyst layer with ionomer/Pt gradient distribution", Materials Today Communications, 40, 109668, 2024. https://doi.org/10.1016/j.mtcomm.2024.109668

[29] Schwarz, D., Djilali, N. "Three-dimensional modelling of catalyst layers in PEM fuel cells: Effects of non-uniform catalyst loading", International Journal of Energy Research, 33, pp. 631–644, 2009. https://doi.org/10.1002/er.1497

[30] Kamarajugadda, S., Mazumder, S. "Numerical investigation of the effect of cathode catalyst layer structure and composition on polymer electrolyte membrane fuel cell performance", Journal of Power Sources, 183(2), pp. 629–642, 2008. https://doi.org/10.1016/j.jpowsour.2008.05.072

[31] Scott, K., Pilditch, S., Mamlouk, M. "Modelling and experimental validation of a high temperature polymer electrolyte fuel cell", Journal of Applied Electrochemistry, 37(11), pp. 1245–1259, 2007. https://doi.org/10.1007/s10800-007-9414-1

[32] Ni, Z., Wang, L., Wang, B. "Unveiling the impact of pore structure of cathode catalyst layer on proton exchange membrane cell performance", International Journal of Hydrogen Energy, 60, pp. 1404–1413, 2024. https://doi.org/10.1016/j.ijhydene.2024.02.303

[33] Larbi, B., Alimi, W., Chouikh, R., Guizani, A. "Effect of porosity and pressure on the PEM fuel cell performance", International Journal of Hydrogen Energy, 38(9), pp. 8542–8549, 2013. https://doi.org/10.1016/j.ijhydene.2012.11.022

[34] Ott, S., Bauer, A., Du, F., Dao, T. A., Klingenhof, M., Orfanidi, A., Strasser, P. "Impact of Carbon Support Meso-Porosity on Mass Transport and Performance of PEMFC Cathode Catalyst Layers", ChemCatChem, 13(22), pp. 4759–4769, 2021. https://doi.org/10.1002/cctc.202101162

[35] Lee, Y., Kim, T. K., Choi, Y. S. "Effect of Porosity in Catalyst Layers on Direct Methanol Fuel Cell Performances", Fuel Cells, 13(2), pp. 173–180, 2013. https://doi.org/10.1002/fuce.201200014

[36] Bing, Y., Liu, H., Zhang, L., Ghosh, D., Zhang, J. "Nanostructured Pt-alloy electrocatalysts for PEM fuel cell oxygen reduction reaction", Chemical Society Reviews, 39(6), pp. 2184–2202, 2010. https://doi.org/10.1039/B912552C

[37] Jia, Q. Liang, W., Bates, M. K., Mani, P., Lee, W., Mukerjee, S. "Activity Descriptor Identification for Oxygen Reduction on Platinum-Based Bimetallic Nanoparticles: *In Situ* Observation of the Linear Composition–Strain–Activity Relationship", ACS Nano, 9(1), pp. 387–400, 2015. https://doi.org/10.1021/nn506721f

[38] Sun, Y., M. Delucchi, M., Ogden, J. "The impact of widespread deployment of fuel cell vehicles on platinum demand and price", International Journal of Hydrogen Energy, 36(17), pp. 11116–11127, 2011. https://doi.org/10.1016/j.ijhydene.2011.05.157

[39] Quintech "Quintech.de", [online] Available at: https://www.quintech.de/en/produkte/components/catalysts/c-60-pt-ac-2/?utm_source=chatgpt.com [Accessed: 24 June 2025]

[40] Jalali, S., Seyedghayem, M., Saboor, F., Venkatramani, A., Asgari, M. "Proton Exchange Membrane Fuel Cells: Focused onOrganic-Inorganic Nanocomposite Membranes", Periodica Polytechnica Chemical Engineering, 67(3), pp. 472–489, 2023. https://doi.org/10.3311/PPch.21632

[41] Shao, S., Cheng, Y., Duan, W., Wang, W., Lin, Y., Wang, Y., Liu, J. "Nanostructured Electrocatalysts for PEM Fuel Cells and Redox Flow Batteries: A Selected Review", ACS Catalysis, 12(5), pp. 7288–7298, 2015. https://doi.org/10.1021/acscatal.5b01737

[42] Bharath, Y., Ankireddy, S. B., Naidu, S. V. "The Performance of PEM Fuel Cell Using Platinum- Ruthenium Alloy Catalyst With Variable Catalyst Loading", IJSART, 7(11), pp. 40–48, 2021.

[43] Du, S., Millington, B., Pollet, B. G. "The effect of Nafion ionomer loading coated on gas diffusion electrodes with in-situ grown Pt nanowires and their durability in proton exchange membrane fuel cells", International Journal of Hydrogen Energy, 36(7), pp. 4386–4393, 2011. https://doi.org/10.1016/j.ijhydene.2011.01.014

[44] Chen, H., Song, Z., Zhao, X., Zhang, T., Pei, P., Liang, C. "A review of durability test protocols of the proton exchange membrane fuel cells for vehicle", Applied Energy, 224, pp. 289–299, 2018. https://doi.org/10.1016/j.apenergy.2018.04.050

[45] Carcadea, E., Varlam, M., Marinoiu, A., Raceanu, M., Ismail, M. S., Ingham, D. B. "Influence of catalyst structure on PEM fuel cell performance e A numerical investigation", International Journal of Hydrogen Energy, 44(25), pp. 12829–12841, 2019. https://doi.org/10.1016/j.ijhydene.2018.12.155

[46] Pivac, I., Bezmalinović, D., Barbir, F. "Catalyst degradation diagnostics of proton exchange membrane fuel cells using electrochemical impedance spectroscopy", International Journal of Hydrogen Energy, 43(29), pp. 13512–13520, 2018. https://doi.org/10.1016/j.ijhydene.2018.05.095

[47] Sanchez, D., Ruiu, T., Biswas, I., Friedrich, K., Sanchez-Monreal, J., Vera, M. "Effect of the Inlet Gas Humidification on PEMFC Behavior and Current Density Distribution", ECS Transactions, 64, pp. 603–617, 2014. https://doi.org/10.1149/06403.0603ecst

[48] Zhang, Q., Tong, Z., Ting, S., Cheng, Z. "Self-humidifying effect of air self-circulation system for proton", Renewable Energy, 164, pp. 1143–1155, 2021. https://doi.org/10.1016/j.renene.2020.10.105

[49] Neyerlin, K., Gasteiger, H., Mittelsteadt, C., Jorne, J., Gu, W. "Effect of Relative Humidity on Oxygen Reduction Kinetics in a PEMFC", Journal of The Electrochemical Society, 152, A1073, 2005. https://doi.org/10.1149/1.1897368

[50] Xie, N., Wei, W., Ba, J., Yang, T. "Operation parameters study on the performance of PEMFC based orthogonal test method", Case Studies in Thermal Engineering, 61, 105035, 2024. https://doi.org/10.1016/j.csite.2024.105035

[51] Lévai, E., Paraicz, P., Szijjártó, G., Bereczky, Á. "Analytical Calculation of the Optimal Temperature and Expected Voltage of a PEM Fuel Cell Considering the Properties of the Membrane Material", Fuel Cells, 25(5), e70021, 2025. https://doi.org/10.1002/fuce.70021

[52] Shinagawa, T., Garzia-Esparza, A., Takanabe, K. "Insight on Tafel slopes from a microkinetic analysis of aqueous electrocatalysis for energy conversion", Scientific Reports, 5(1), 13801, 2015. https://doi.org/10.1038/srep13801

[53] Sosna, B., Korup, O., Horn, R. "Probing local diffusion and reaction in a porous catalyst pellet", Journal of Catalysis, 381, pp. 285–294, 2020.
https://doi.org/10.1016/j.jcat.2019.11.005

[54] Kriston, Á., Popov, B. "Analysis of the Effect of Pt Loading on Mass and Specific Activity in PEM Fuel Cells", Journal of The Electrochemical Society, 160(4), pp. 406–412, 2013.
https://doi.org/10.1149/2.075304jes

[55] Halvorsen, I. J., Pivac, I., Bezmalinović, D., Barbir, F., Zenith, F. "Electrochemical low-frequency impedance spectroscopy algorithm for diagnostics of PEM fuel cell degradation", International Journal of Hydrogen Energy, 45(2), pp. 1325–1334, 2020.
https://doi.org/10.1016/j.ijhydene.2019.04.004